

frontpage

assignment 1/2

assignment 2/2

ACKNOWLEDGEMENT

text....

SUMMARY

Text in English.

keywords:

text, text, text

SOUHRN

Text.

klíčová slova:

text, text, text

Contents

1 INTRODUCTION	1
1.1 Studied compounds	2
1.1.1 Polylactic acid	2
1.1.2 Active pharmaceutical ingredients	2
1.2 Objective	3
2 THEORETICAL PART	5
2.1 Force fields	5
2.1.1 OPLS	7
2.1.2 Polarizable Force Fields	7
2.2 Molecular dynamics	7
2.2.1 Verlet integration	8
2.2.2 Velocity Verlet	9
2.2.3 Constraint dynamics	9
2.2.4 SHAKE algorithm	9
2.3 title	10
3 COMPUTATIONAL METHODS	11
4 RESULTS AND DISCUSSION	13
4.1 Simulations of API	13
4.2 Simulations of mixtures of APIs and PLA	13
4.2.1 Calculated properties of mixtures	13
4.2.2 Glass transition temperature	13
4.2.3 Radial distribution functions	14
4.2.4 Diffusion coefficients	20
4.3 Smesi s polarizovany m polem	22
5 CONCLUSION	23
REFERENCES	24
List of Abbreviations	27
List of Symbols	28
List of Tables	29

List of Figures	30
Appendix A Headline	32

1 INTRODUCTION

In crystalline forms, most of the newly discovered active pharmaceutical ingredients (APIs) are poorly soluble in water, which limits their bioavailability, dissolution, and then their distribution through the organism. This fact limits potential wider use of numerous API as a solid drug in medical treatment. Today, combinatorial chemistry techniques and high-throughput screening have led to a sharp increase in the quantity of proposed nonsoluble API molecules, so the oral administration of poorly soluble drugs has become the biggest challenge for formulation scientists in the pharmaceutical industry. [1] There are different strategies to overcome this issue, such as cocrystal formation [2], conversion of an API to its salt [3] or using dispersions of API in various matrices. [4]

In 1961, Sekiguchi and Obi provided the earliest account of the so-called first-generation solid dispersion, when they discovered that the creation of eutectic mixtures enhances the rate of drug release and bioavailability. First-generation solid dispersions were built from crystalline carriers such as urea or sugars, forming crystalline solid dispersions. The second generation of solid dispersions is based on replacing crystalline carriers by amorphous carriers such as polymers, forming an amorphous product in which API is dissolved. There exist also a third generation of solid dispersions using a surfactant carrier or a combination of amorphous polymers and surfactants. [5]

The aim of researchers is to overcome the poor solubility of APIs by using amorphous solid phases of APIs and to avert the rearrangement of their molecules into a crystal lattice. However, crystalline forms of APIs are advantageous because of their better stability during long-term storage and more reliable predictions of material properties at the molecular level under defined conditions. [6] The better solubility of APIs in amorphous forms comes from a higher Gibbs energy of the amorphous form compared to the crystalline forms. During processing, storage, and after contact with water or humidity, the thermodynamically metastable amorphous forms tend to crystallise. Solid mixtures of API and excipients (e.g. polymeric excipients) create amorphous solid dispersions (ASD) and offer a way to inhibit crystallisation of the API before and after oral administration of the dose. [7]

The creation of an amorphous dispersion of an API can generally have a twofold effect on the rate of solid-state crystallisation, affecting both thermodynamic and kinetic aspects. Thermodynamically, it reduces the Gibbs energy of the dispersion due to strong beneficial intermolecular interactions between API and its excipient, as well as it increases kinetic barriers to recrystallisation. On the atomic scale of

individual interactions stabilizing such solid dispersions, hydrogen bonding makes the most significant contribution. [8]

Other suitable biocompatible and biodegradable polymers for ASD could be polyethylene glycol (PEG) and polyvinylpyrrolidone (PVP). [9]

1.1 Studied compounds

1.1.1 Polylactic acid

Polylactic acid (PLA) was chosen as a biocompatible polymer excipient. PLA is a biodegradable polymer formed by the polymerisation of lactic acid. The formula of the PLA monomer unit is shown in Figure 1. In this work, two condensed units of D-PLA were considered as the simplest building block for creating all of the other longer polymer chains. Polymer samples of a length up to 100 dimer units were created by replicating these dimer units. The molar weight of our dimer unit considered in the investigation is $M_w = 162.14 \text{ g mol}^{-1}$, which means that the longest polymer chain used in the simulations has a molar weight equal to $M_w = 14\,431 \text{ g mol}^{-1}$

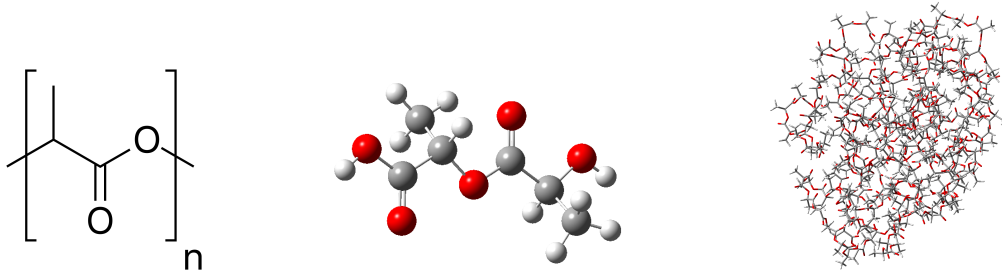


Figure 1: PLA formula on the left, PLA dimer block representing the chain unit used to build up polymer chain in the middle and a folded PLA chain containing 100 dimer block used to create mixtures with APIs on the right.

1.1.2 Active pharmaceutical ingredients

The first selected API is **ibuprofen**, systematically 2-(4-Isobutylphenyl)propanoic acid ($C_{13}H_{18}O_2$) as an example of a widely used analgesic, antipyretic, anti-inflammatory drug. The racemic mixture of ibuprofen is commonly used in medical treatment. The S-enantiomer has a stronger pharmaceutical activity than the R-enantiomer, which is metabolically transformed to S-form in the organism. [10] In this work the S-form, which is visualised in Figure 2, is used. The molar weight of ibuprofen is $M_w = 206.28 \text{ g mol}^{-1}$ and the melting temperature of the enantiopure crystal is 324.4 K. [11]

The second selected API is **naproxen**, systematically 2-(6-Methoxynaphthalen-2-yl)propanoic acid ($C_{14}H_{14}O_3$), a non-steroidal anti-inflammatory drug, used as a

painkiller. Naproxen contains three oxygen atoms (one carboxyl group and one ether bond), the structure is shown in Figure 2 in the upper right corner. On the basis of its structure, naproxen can donate one hydrogen bond and accept up to six hydrogen bonds, steric factors limits the actual coordination. Naproxen is a white crystalline powder, with a molar weight of $M_w = 230.263 \text{ g mol}^{-1}$ and melting temperature is 429.3 K. [11]

Carbamazepine, alternatively 5-Carbamoyl-5H-dibenzo(b,f)azepine ($C_{15}H_{12}N_2O$) is a representative anticonvulsant, which is used for the treatment of seizures and neuropathic pain. Carbamazepine contains two nitrogen atoms (amide group) and one oxygen in the carbonyl group; its structure is shown in Figure 2 on the left side. According to its structure, carbamazepine can theoretically accept up to two hydrogen bonds and donate up to four hydrogen bonds. Carbamazepine is a white crystalline powder, with a molar weight of $M_w = 236.273 \text{ g mol}^{-1}$ and melting temperature of 463.6 K. [11]

Indomethacin, 2-1-[(4-Chlorophenyl)carbonyl]-5-methoxy-2-methyl-1H-indol-3-ylacetic acid ($C_{19}H_{16}ClNO_4$), whith structure depicted in Figure 2, is used in the treatment of musculoskeletal and joint disorders. The molar weight is $M_w = 357.8 \text{ g mol}^{-1}$ and the melting temperature is 433.3 K. [11]

The last selected API was **sulfathiazole** with systematic name 4-amino-N-thiazol-2-ylidenebenzene-sulfonamide as a representative antibiotic drug from the sulfonamides group, which is used in the treatment of pyogenic cutaneous infections. Sulfathiazole is a white crystalline powder, with a molar weight (M_w) = 255.3 gmol^{-1} , which is highly polymorphic, five polymorphs have been discovered so far [6]. All known polymorphs of sulfathiazole crystallise in the $P2_1/c$ space group, but there are differences in intermolecular bonding and structural properties [12]. The II polymorph structure, shown in Figure 3, is used in this work. There are four molecules of sulfathiazole in the crystal monoclinic unit cell.

1.2 Objective

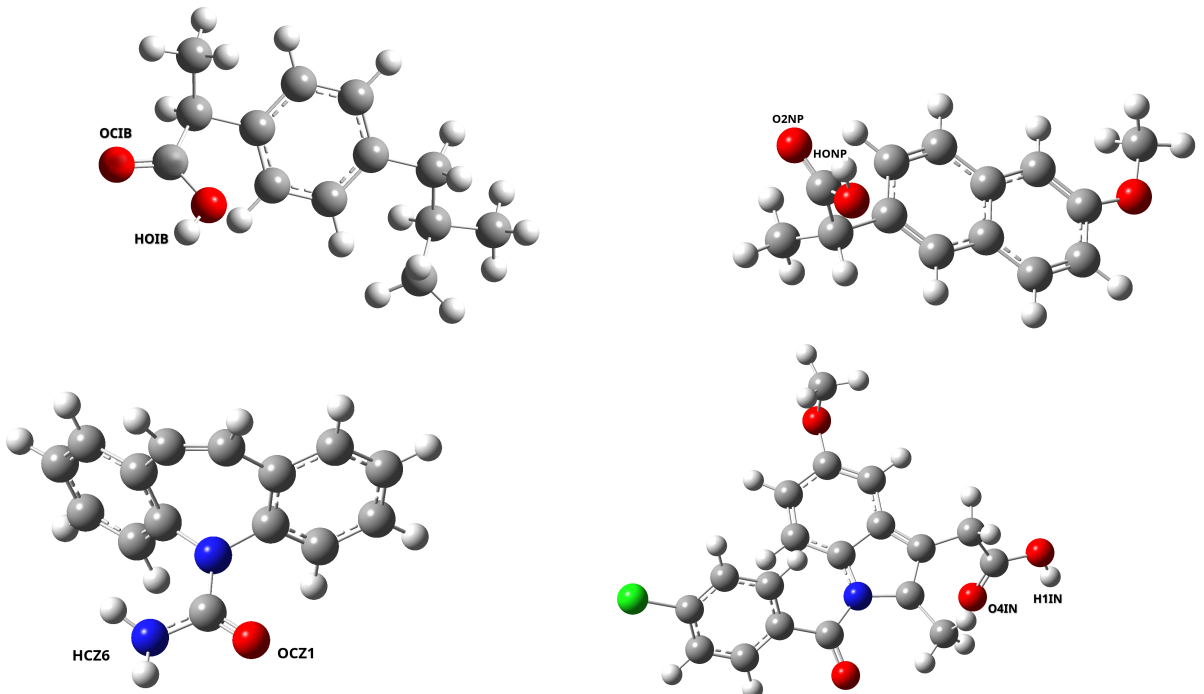


Figure 2: Molecular structures of ibuprofen (**top left**), naproxen (**top right**), carbamazepine (**bottom left**) and indomethacin (**bottom right**). Atom types contributing most to the hydrogen bonding are tagged for each molecule.

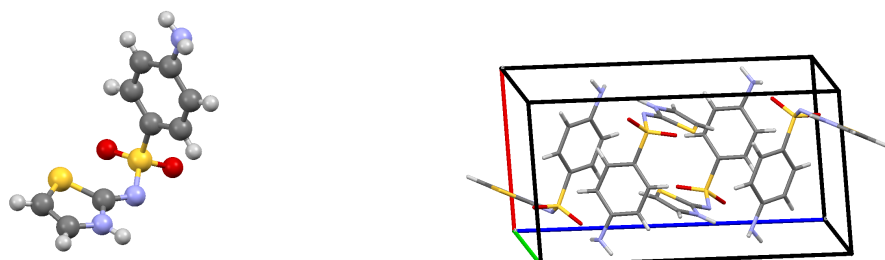


Figure 3: Sulfathiazole - molecular structure on the left and a unit cell of its II polymorph on the right.

2 THEORETICAL PART

In order to convert a real system consisting of individual molecules into a form that can be understood by a computer software, we must define individual parameters that are essential for describing mutual interactions of atoms. When describing real systems, it is usually necessary to consider a certain degree of approximation due to the possible computational complexity. In computational chemistry methods, we often encounter the so-called Born-Oppenheimer approximation, which is based on the decoupling of the motion of nuclei and electrons. The basis of the approximation is the orders-of-magnitude difference in mass between the electron and the nucleus. The latter thus move very slowly relative to the electrons and can thus be considered as a fixed point charge. This allows us to calculate the energy of a molecule as a function of the positions of the nuclei, in quantum chemistry we talk about the so-called Potential Energy Surface (PES), which is a function of $3N$ coordinates, where N is the number of nuclei. [13]

For small systems it is possible to calculate the PES based on quantum chemistry methods using reasonable resources, for very large systems this is not yet realistic. We therefore introduce a classical-mechanics set of analytic functions, yet empiric parameters called the Force Field (FF), which enable to evaluate the energy of simulated systems depending on the positions of the nuclei. Methods based on the use of such Force Fields are called molecular mechanics, which are applied especially when quantum phenomena are not of great importance and we can use classical mechanics approach or big amorphous systems where quantum-based calculations would be extremely expensive and resource taking. [14]

2.1 Force fields

The total energy calculated using the force field can be broken down into two contributions, a binding and a non-binding term, which are further expanded in Equations 2.1 and 2.2.

$$E_{\text{bonded}} = E_{\text{bond}} + E_{\text{angle}} + E_{\text{torsion}} \quad (2.1)$$

$$E_{\text{nonbonded}} = E_{\text{electrostatic}} + E_{\text{Van der Walls}} \quad (2.2)$$

To get a better idea of what lies behind the individual terms, visualization of

the corresponding mechanistic degrees of freedom is in the Figure 4. OBRÁZEK VYTVOŘÍM VLASTNÍ V PODOBNÉM DUCHU—

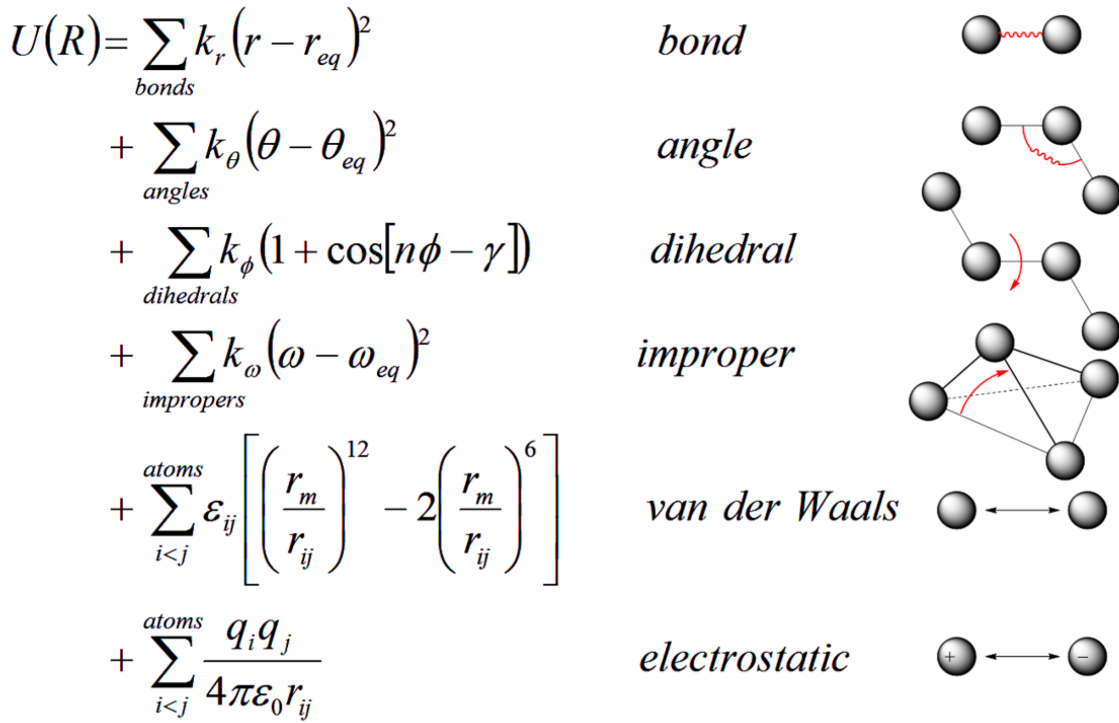


Figure 4: caption

By the level of functional description (number of terms) of the interactions in the force field, we distinguish force fields of three classes. Class 1 force fields contain the 5 terms mentioned in the two equations above (bond, angle, torsion, Lennard-Jones and electrostatic), examples of such FF are the DREIDING, AMBER, GAFF and OPLS. In addition, class 2 force fields include bond-bond and bond-angle coupling terms, anharmonic terms simultaneously with all class 1 terms, examples of such fields are PCFF or ReaxFF. The third class includes fluctuations of charge distribution in time (charge polarization effect), and they are called polarizable FF. [15]

During the parameterization of force fields (FF), we start from the assumption of transferability, similar chemical groups of different molecules interact in the same way. When constructing a force field for large molecules, we can use parameters obtained from data for small molecules, which are much more easily graspable and contain the same functional groups. [14] In model development, our aim is to achieve the most universal description of the system while still closely corresponding to its actual state. This can be facilitated by employing higher-order terms; however, incorporating anharmonic and cross terms introduces the need for a greater amount of FF parameters. We strive to avoid situations where we employ an overly adapted and detailed model that merely reproduces inserted information without providing any predictive capabilities. [15]

According to the level of parameterization, there are 3 basic types of force fields. In the first case, where the parameters are determined for each individual atom in the system, including hydrogens, we speak of an all-atom force field. A united atom force field is one where we parameterize the individual functional groups (interaction centers), such an interaction center could be for example a methyl group. The third type of force field is coarse grained, used mainly for protein and polymer simulations, offering higher computational efficiency for long simulations of large molecules by grouping them into "superatoms". [16]

2.1.1 OPLS

2.1.2 Polarizable Force Fields

2.2 Molecular dynamics

The molecular dynamics method is based on solving the equations of motion of classical Newtonian mechanics for atoms. Let us choose the assumption that the interaction potential U is continuous and differentiable. The force acting on the i

particle can thus be written as an equation 2.3

$$f_i = -\frac{\partial U(r^N)}{\partial r_i}, \quad i = 1, \dots, N. \quad (2.3)$$

In molecular dynamics, we are focused on the time development of the model. In other words, we are looking for the trajectory of the solution of the respective systems of differential equations. In Newtonian mechanics, acceleration is directly related to forces through the equations of motion. Formally, we can write the equation 2.4

$$\ddot{r}_i = \frac{f_i}{m_i}, \quad i = 1, \dots, N, \quad (2.4)$$

where the second time derivative of the positions appears on the left side. The equation 2.4 is a system of $3N$ ordinary differential equations for a set of N atoms. As initial conditions, we usually choose the knowledge of all atomic positions r_i and velocities \dot{r}_i at the initial time $t = t_0$.

We solve equation 2.4 using the finite difference method when we track the desired solution in the form of the function $r_i(t), i = 1, \dots, N$, in the time interval $[t_0, t_{max}]$ at discrete points of the form $t = t_0 + kh$, where h is the integration step and k is a non-negative integer.

To find a solution, it is necessary to calculate the forces acting on individual particles at each step of the simulation. One of the methods that is applied in this area is the Verlet integration method. It is a simple and very effective method that provides sufficiently accurate results in the physico-chemical context. Its great advantage is the time-reversibility and the conservation of the total energy of the system [17].

2.2.1 Verlet integration

Verlet integration method is a numerical method for integrating the equation 2.3. We express the second derivative using finite differences. From the second-order Taylor expansion $r_i(t \pm h)$ centred at t , we obtain the formula

$$\ddot{r}_i = \frac{r_i(t-h) - 2r_i(t) + r_i(t+h)}{h^2}, \quad (2.5)$$

binding values at three points in a row ($t-h$, t and $t+h$). We will use this characteristic to calculate $r_i(t+h)$. By substituting 2.5 into 2.3 we get

$$r_i(t+h) = 2r_i(t) - r_i(t-h) + h^2 \frac{f_i(t)}{m_i}. \quad (2.6)$$

In this formulation, we are able to calculate the new positions at time $t + h$ from knowledge of the forces at time t , the positions of the particles at time t and the previous time $t - h$. The time reversibility of the method is clearly visible here. The advantage is that the force is calculated only once in each step of the simulation. For the position preceding the initial position ($r_i(t_0 - h)$), we can use the expansion 2.7

$$r_i(t_0 - h) = r_i(t) - h\dot{r}_i(t_0) + h^2 \frac{f_i(t_0)}{2m_i}. \quad (2.7)$$

2.2.2 Velocity Verlet

2.2.3 Constraint dynamics

When integrating equations of motion, we often impose constraints on certain aspects of molecular geometries. The main reason is to enable using a longer simulation time step. If we simulate with a too large time step, we introduce large errors into the simulations, leading in extreme cases to a crash of the simulation. The calculated particle positions at time $t + h$ may lead to overlapping of particles, the calculated force acting on the particles may divert from physically reasonable configurations. Conversely, the use of inappropriately short simulation steps reduces the efficiency of the simulations (the most computationally and therefore time consuming element of the simulations is the calculation of the forces when integrating the equations of motion). [17] The criterion determining the optimal step length is the accuracy of the conservation of total energy. The step length can be determined by an Nyquist sampling theorem that says that the time step must be half or less of the period of the quickest dynamics exhibited in the system. Thus, for systems containing very light hydrogen atoms, we can either artificially increase the mass of the hydrogen atom while redistributing the masses of the other molecules to conserve the overall mass of the molecule, or fix the bond angles or bond lengths terminating in the hydrogen atoms. It is the fixation of hydrogen bond lengths that is most often implemented in the Verlet method, using an algorithm called SHAKE. Fixing the bond length allows us to use a longer time step (we are no longer limited by the motion of very light particles) and, unlike fixing angles, does not introduce large deviations in the simulations.

2.2.4 SHAKE algorithm

The SHAKE algorithm is based on Verlet's integration method and is iterative. The first step is to initialize the initial velocities and positions of the atoms, then calculate the positions using Verlet's method without considering bond length constraint. We

then create the λ correction of the atom positions to constrain the bond length, which we calculate by considering the correct bond length between atoms i and j from the condition TUTO ČÁST UPRAVÍM ABY tam nebyly zbytečné rovnice

$$[\vec{r}_{\text{Verlet},ij}(t+h) - \lambda \vec{r}_{ij}(t)]^2 = \vec{r}_{ij}(t)^2, \quad (2.8)$$

where Verlet index comes from previously described Equation 2.6 for Verlet method. When we consider After omitting the we can calculate λ as

$$\lambda \approx \frac{|\vec{r}_{\text{Verlet},ij}(t+h)|^2 - |\vec{r}_{ij}(t)|^2}{2\vec{r}_{\text{Verlet},ij}(t+h) \cdot \vec{r}_{ij}(t)} \quad (2.9)$$

$$\vec{r}_i(t+h) = \vec{r}_{\text{Verlet},i}(t+h) + \lambda \frac{1/m_i}{1/m_i + 1/m_j} \vec{r}_{ij} \quad (2.10)$$

$$\vec{r}_j(t+h) = \vec{r}_{\text{Verlet},j}(t+h) - \lambda \frac{1/m_j}{1/m_i + 1/m_j} \vec{r}_{ij} \quad (2.11)$$

2.3 title

3 COMPUTATIONAL METHODS

LAMMPS software [18] (version 5 May 2020) was used for all molecular dynamics calculations. The placement of molecular chains in the simulation boxes was done by Packmol [19], the chains were randomly distributed in the space of a cubic box. The input files for the LAMMPS software were generated using the fftool [20] script written in the Python programming language.

We also used periodic boundary conditions in the directions of all axes and the velocity Verlet integrator. Contributions of long-range charge interactions of distant atoms were calculated using the long-range solver using the particle-particle-particle mesh (PPPM) algorithm [21]. The bonds and angles were considered as harmonic oscillators, and for dihedral angles, OPLS (Optimised Potentials for Liquid Simulations) was used for every atom. Coulombic point charges and the Lennard-Jones potential were used, the cut-off distance for dispersion and Coulombic interactions was set to 12 Å. The SHAKE atom algorithm [22] was applied to constrain the lengths of covalent bonds that terminate in hydrogen atoms. The simulations were run under *NPT* conditions using the Nosé-Hoover thermostat and barostat [23], with relaxation times for temperature control as 100 fs and pressure control as 1000 fs. The simulations contained around 25 000 atoms in a simulation box. From previous research, this was considered to be a suitable setting. [9]

All-atom non-polarisable force fields were used during MD simulations, the parameterisation of the PLA force field was obtained from the literature [24], the parameterizations of APIs were also taken from the literature. [25]

We started all simulations with an equilibration simulation run from randomly packed simulation boxes under the temperature of 500 K and pressure of 1 bar in three blocks with a gradually increasing time-integration step. The simulation began with an equilibration procedure using a step of 0.25 fs, followed by steps 0.5 and 0.75 each for a simulation time of 0.5 ns, then 1 ns of simulation with a step of 1 fs. From this point, we cooled the system, down to 300 K for 2 ns with a step of 1 fs. After this cooling, we continued with a 10 ns long production run with a temperature of 300 K and pressure equal to 1 bar.

From these production runs, we evaluated the MSD (Mean Squared Displacement) of API and PLA molecules in the mixture and the RDF (radial distribution function) of atom interactions. We also performed a production run at the higher temperature of 500 K and the same pressure of 1 bar starting from conformations after

the first equilibration under 500 K. We also sampled RDFs and MSDs. Those simulations were performed for neat APIs, PLA polymer, and mixtures with different concentrations of API. For each API, the concentration ratio API:PLA in terms of the number of molecules in a simulation box was 100:17, 200:17, and 300:17. The corresponding molar and mass fractions are available in the Table 1.

Table 1: The concentration of API in mixtures with PLA, expressed in molar and mass fractions.

N_{API}	N_{PLA}	x_{API}	w_{nap}	w_{cbz}	w_{ibu}	w_{indo}
100	17	0.85	0.086	0.088	0.078	0.13
200	17	0.92	0.16	0.16	0.14	0.23
300	17	0.95	0.22	0.22	0.20	0.30

To determine the glass transition temperature (T_g) of the mixtures, we performed simulated annealing simulations with a gradually decreasing temperature cooling rate (30 K ns⁻¹) starting at 800 K and ending at 200 K. Systems containing a mixture of API and PLA were first heated from 500 K to 800 K over 2 ns. To have statistically more reliable data, simulated annealing simulations were performed from 5 different initial conformations. To obtain those conformations a 4 ns long simulation at 800 K was done sampling atomic coordinates within the image of the box every 1 ns.

4 RESULTS AND DISCUSSION

4.1 Simulations of API

The box of neat carbamazepine contained 800 molecules (24 000 atoms), after equilibration run ($T=500$ K), the size of the box was 66 Å. In the naproxen simulation box 800 molecules were presented (24 800 atoms), balanced box size was 66 Å. For ibuprofen the balanced box size with 800 molecules (26 400 atoms) was 67 Å. The simulation box containing 600 molecules (24 600 atoms) of indomethacine had size of 66 Å.

Table 2: Calculated mixing energies and volumes for API mixtures of different concentrations, simulations under 500 K.

API	N_{API}	N_{atoms}	$l_{\text{box}}, \text{\AA}$
carbamazepine	800	24 000	66
naproxen	800	24 800	66
ibuprofen	800	26 400	67
naproxen	600	24 600	66

COMPARISON OF DENSITIES WITH EXPERIMENTS?

4.2 Simulations of mixtures of APIs and PLA

4.2.1 Calculated properties of mixtures

Mixing energies and volumes were calculated for both systems, and the comparison is shown in Table 3. The data show that a mixture of naproxen and PLA can create a more advantageous arrangement of molecules in space, meaning that the mixing volumes are negative. For carbamazepine the trend is the opposite; this could be caused by the shape of the carbamazepine molecule when the mixture needs more space. From the positive changes in energies, we can assume that mixing the APIs with PLA can reduce the interactions between API-API molecules, and also that new interactions between API and PLA are not developed in order to compensate for the API-API cohesion.

4.2.2 Glass transition temperature

The glass transition temperatures of the mixtures were evaluated from the simulated annealing simulations by fitting a hyperbola to the temperature-density data. The

Table 3: Calculated mixing energies and volumes for API mixtures of different concentrations, simulations under 500 K.

API	x_{API}	$V_{\text{m, mixing}}, \text{cm}^3/\text{mol}$	$E_{\text{m, mixing}}, \text{kJ/mol}$
carbamazepine	0.85	0.97	4.79
	0.92	0.48	3.17
	0.95	0.21	2.68
naproxen	0.85	-7.07	7.50
	0.92	-8.50	6.24
	0.95	-9.85	4.75

whole methodology is described in the paper written by Alzate-Vargas[26], the main equation of the fit is Equation 4.1

$$\rho(T) = \rho_0 - a(T - T_0) - b \left[\frac{1}{2}(T - T_0) + \sqrt{\frac{(T - T_0)^2}{4} + e^c} \right]. \quad (4.1)$$

Since this method is sensitive to the initial state of the simulated box, more simulated data starting from different conformations must be provided to evaluate T_g . In this work we used 5 simulations from different initial states.

The resulting value for carbamazepine is $T_{g, \text{cbz}} = 385 \pm 4$ (k = 2) and for naproxen is $T_{g, \text{nap}} = 365 \pm 2$ (k = 2).

4.2.3 Radial distribution functions

Then, all RDFs of mixtures containing the API-API interaction were scaled onto the pure API RDF signal for better visualisation using the following Equation 4.2

$$\text{RDF}_{\text{scaled}} = \text{RDF} \cdot \frac{\frac{V_{\text{API}}}{N_{\text{API}}}}{\frac{V_{\text{mix}}}{N_{\text{mix}}}}, \quad (4.2)$$

where V_{API} is the average volume of the pure API simulation box, N_{API} is the number of molecules in the pure API simulation box and, respectively, for mixtures.

Sampling the radial distribution function from the simulations was done to explore the interactions that are having the highest impact. The hydrogen bonds were mostly studied. All RDF data containing the API-API interaction in the mixtures

were scaled for the intensities of the pure API signal. The strongest API-API interaction was chosen and plotted to study the change between simulations with different concentrations of PLA.

For ibuprofen, the interaction between hydrogen from OH group and oxygen from OC was studied. For naproxen, the hydrogen bonding between two carboxyl groups was studied, for carbamazepine, hydrogen bonding was studied between the NH₂ and OC group and for indomethacine the interaction of oxygen from OC and hydrogen from OH was studied. The selected atom types involved in interactions are visualised in Figure 2.

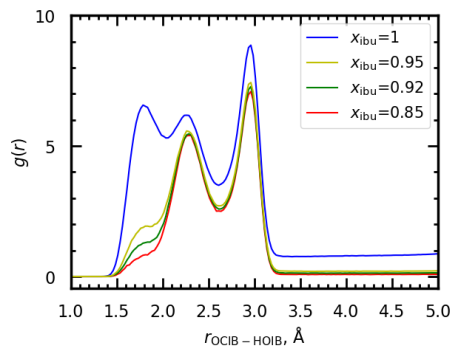


Figure 5: Radial distribution function of the API-API interaction between HOIB hydrogen atom bonded on oxygen and OCIB oxygen atom in a mixture of ibuprofen and PLA for different concentration normalized on values for pure ibuprofen, temperature of 300 K in the left upper corner and 500 K bottom left, coordination numbers on the right.

The RDF of the selected interaction of naproxen is shown in Figure 8. Here is the situation very different, the height of the first peak changes for different concentrations of PLA. For the higher concentration of PLA, the occurrence of the two hydrogen bonds carboxyl group contact is less important, and the contact of the groups is made only by one hydrogen bond.

The RDF of the hydrogen bonding interaction of carbamazepine is shown in Figure 7. The shape and signal response of the peaks for the mixtures are similar for both temperatures, meaning that the impact of the concentration of PLA on the cohesion of carbamazepine in the mixture is very low.

The hydrogen bonding between API and PLA was also studied. The contact visualization is available in Figure 9.

The RDF of hydrogen bonding with the carbonyl group is shown in Figure 10. For carbamazepine, those interactions are weak, we can see that the intensity of the

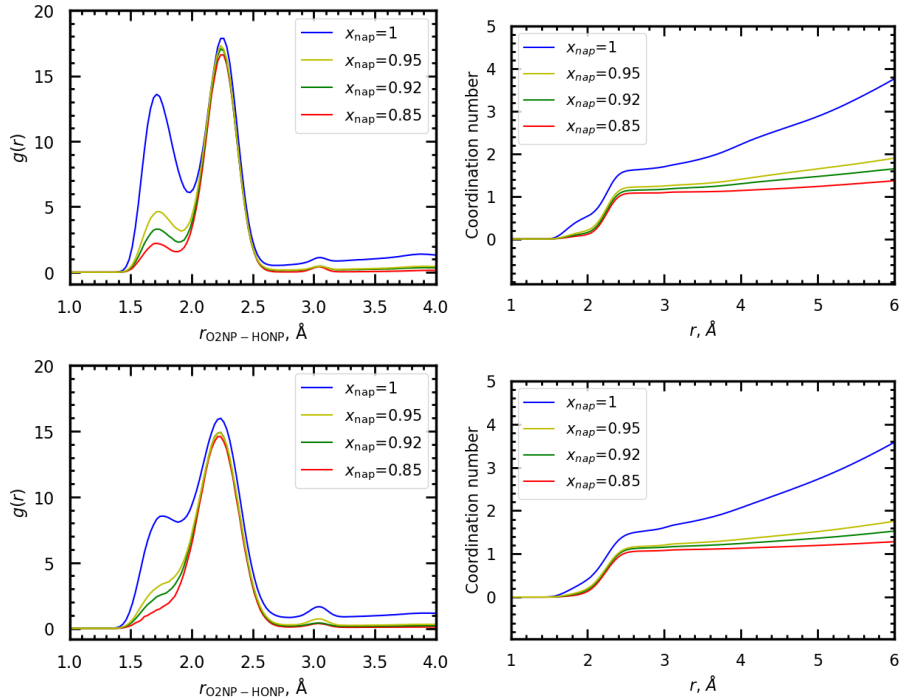


Figure 6: Radial distribution function of the API-API interaction between HONP hydrogen atom and O2NP oxygen atom from COOH group in a mixture of naproxen and PLA for different concentration normalized on values for pure naproxen, temperature of 300 K in the left upper corner and 500 K bottom left, coordination numbers on the right.

first peak is really low. Under temperature 300 K slightly above one, but for 500 K the peak is below one, meaning that this interaction occurs less at a small distance than in the rest of the system. The value converges to one in a long distance. For naproxen, the interaction is more relevant, and the intensity of the peak is much higher but still less than in the NAP-NAP interactions.

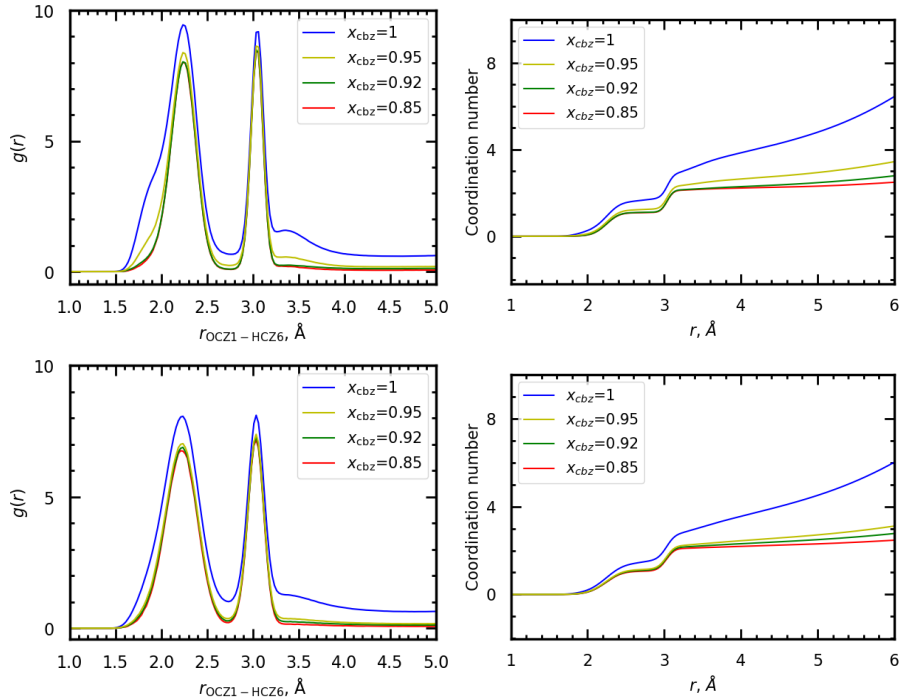


Figure 7: Radial distribution function of the API-API interaction between HCZ6 hydrogen atom bonded on nitrogen and OCZ1 oxygen atom in a mixture of carbamazepine and PLA for different concentration normalized on values for pure carbamazepine, temperature of 300 K in the left upper corner and 500 K bottom left, coordination numbers on the right.

The hydrogen bonds with the oxygen bonded by ether bond in PLA are shown in Figure 11. Here is the same situation as in the previous contact with carbonyl oxygen, but for naproxen, the interaction is less relevant. Both values also converge to 1 in a long distance.

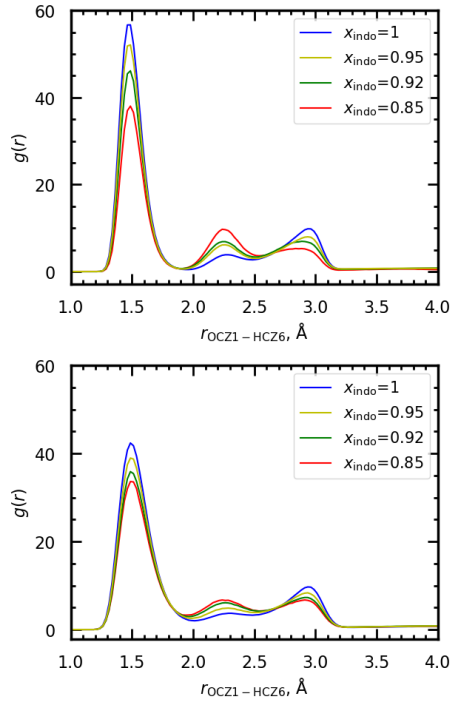
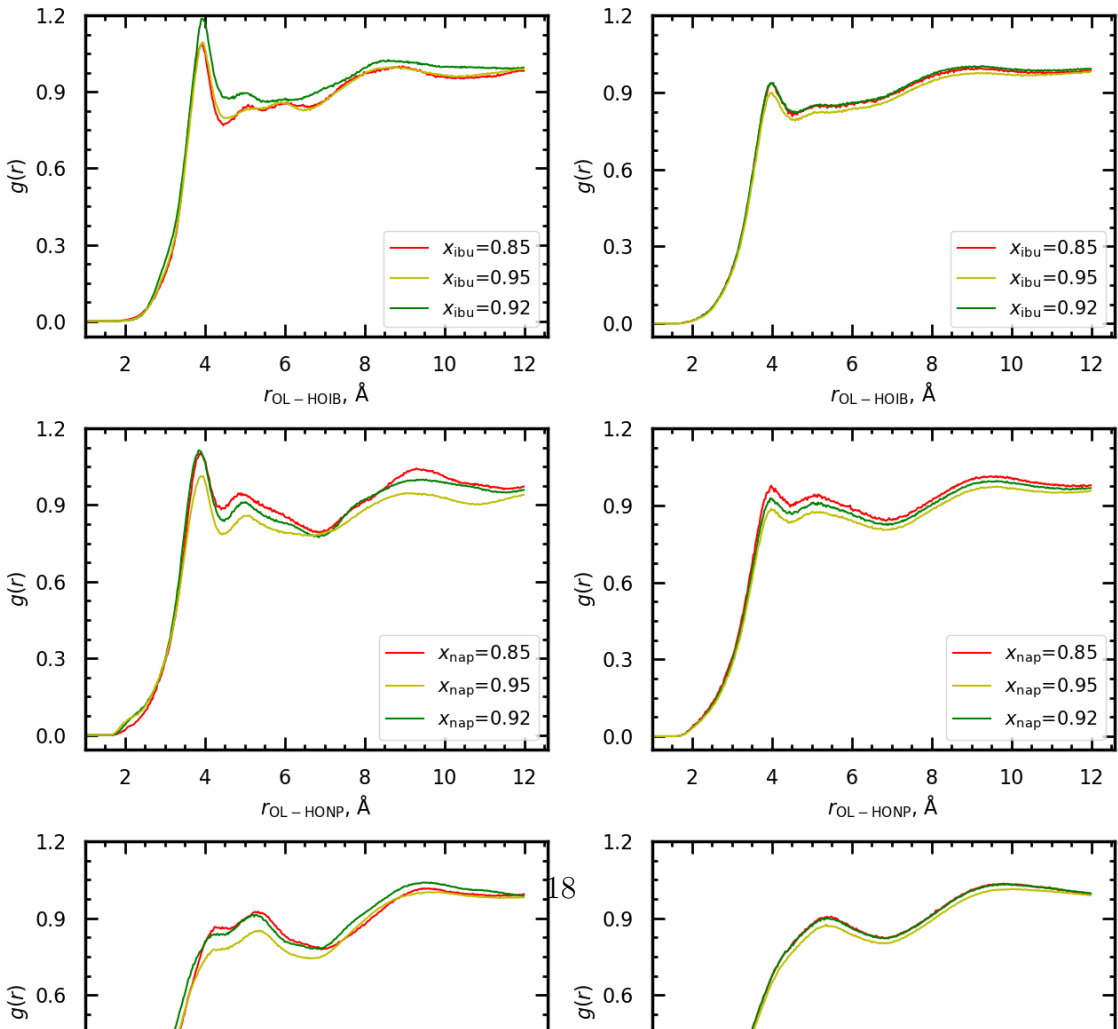


Figure 8: Radial distribution function of the API-API interaction between HCZ6 hydrogen atom and OCZ1 oxygen atom from COOH group in a mixture of indomethacine and PLA for different concentration normalized on values for pure indomethacine, temperature of 300 K in the left upper corner and 500 K bottom left, coordination numbers on the right.



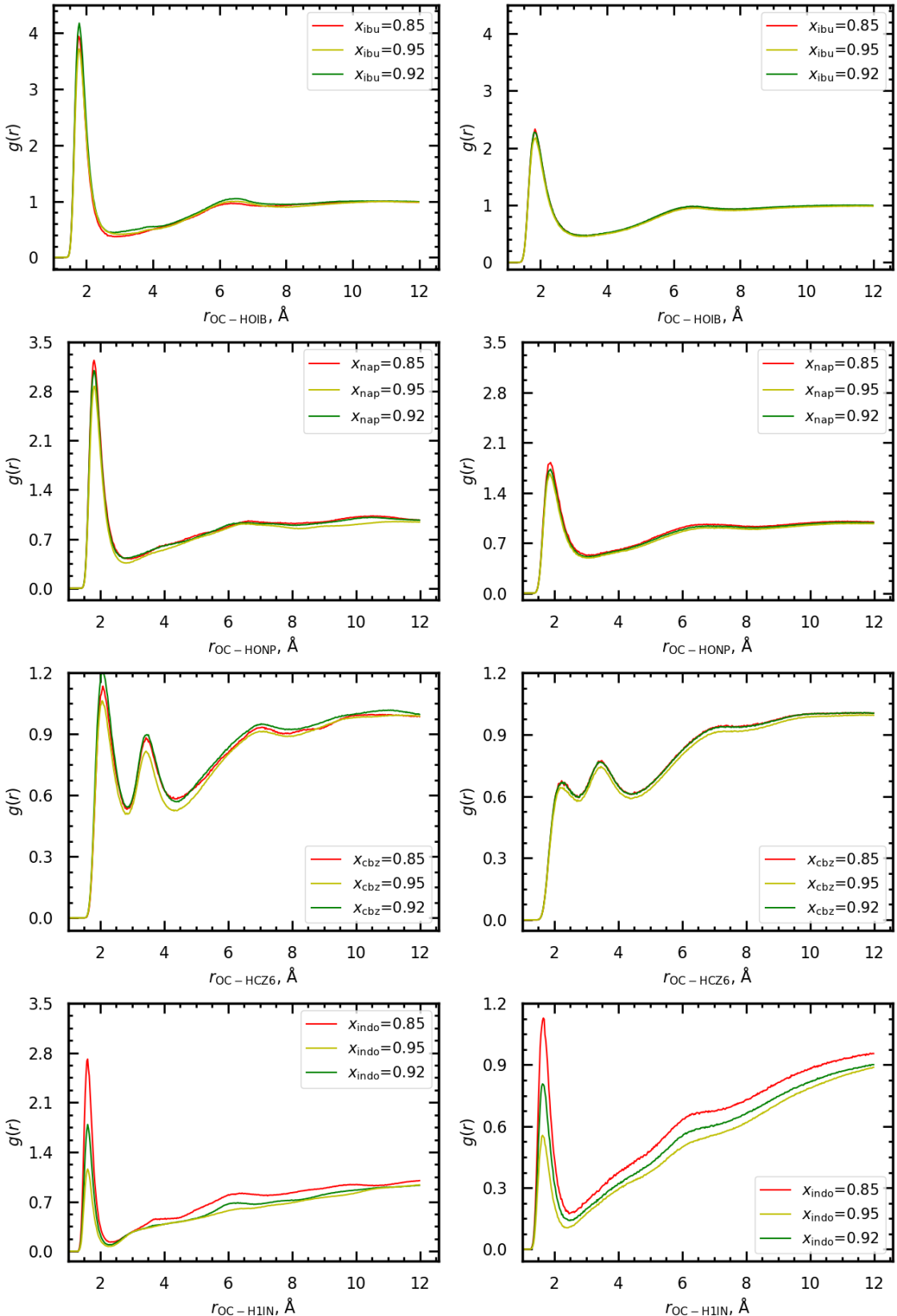


Figure 10: Radial distribution function of the interaction between hydrogen atoms and oxygen atom from carbonyl group in PLA, first ibuprofen on top, second naproxen, third carbamazepine and indomethacine in the bottom, temperature 300 K on the left and 500 K on the right.

4.2.4 Diffusion coefficients

The MSDs were sampled from the 10 ns long run simulations every 1000 fs (integration step 1 fs). At each sampled time step, obtained MSD data were averaged over all API molecules and then plotted as a function of simulation time. The MSD dependencies were then interpolated by a linear functions and related self-diffusivities of the API in the mixtures were evaluated from the slope of the line using the following Equation 4.3

$$D_{\text{API}} = \frac{a}{2d}, \quad (4.3)$$

where D is the diffusion coefficient, a is the slope of the line and d is the dimensionality of the trajectory (3 in our case).

The MSD data for APIs in mixtures with PLA for $T=500$ K are plotted in Figure 12. For ibuprofen, there is a significant difference between mobility of neat API and API mixed within the polymer. This could be result of very strong API-PLA interaction forming in the mixture. The data of carbamazepine shows that with increasing API concentration, mobility also increases. There is also not that enormous difference between neat API. For naproxen, it seems that there is no change for different concentrations of mixtures, also in neat API the mobility is higher. The situation for indometacine is completely different. For neat API the mobility is really low compared to mixtures with PLA. This behaviour seems strange, the reason could be, that in pure API, there are really strong API-API interactions that decrease the mobility. Also the MSD values are much lower.

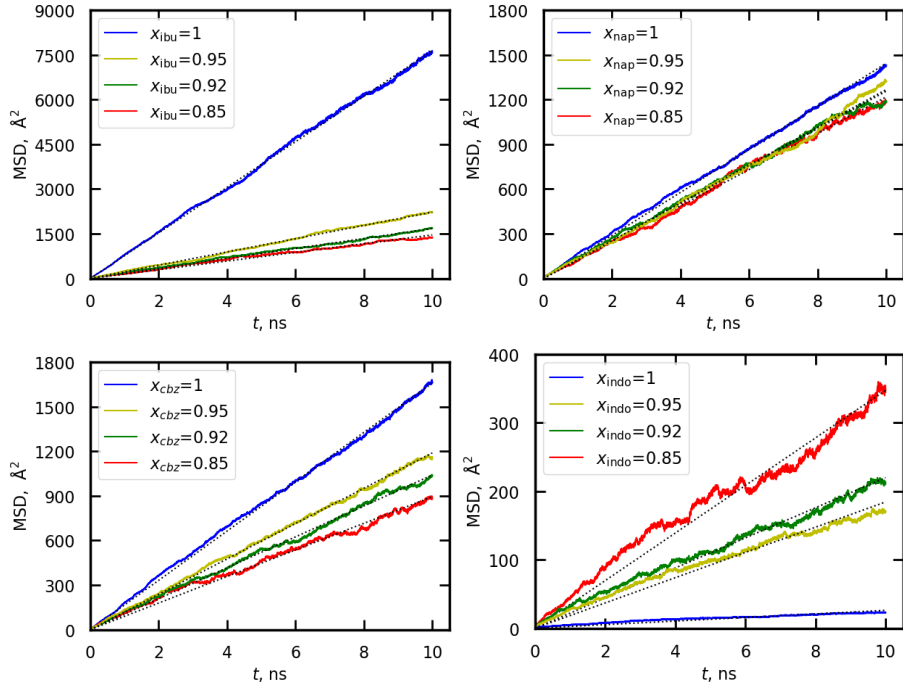


Figure 12: MSD from simulations under 500 K, ibuprofen (**top left**), naproxen (**top right**), carbamazepine (**bottom left**) and indomethacin (**bottom right**).

Self-diffusivities were evaluated from the above data and plotted in Figure 13. The data reveal that in pure liquid carbamazepine the diffusion is faster than in naproxen. For higher temperatures, the main factor affecting diffusion is the shape of the molecules, not the strength of the intermolecular interactions. This is caused because the kinetic energy is higher than the potential for higher temperatures.

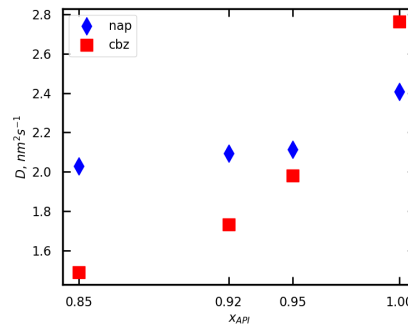


Figure 13: Self-diffusivities for carbamazepine and naproxen as a function of their concentration in the mixtures, temperature 500 K.

MSD was also evaluated at a lower temperature of 300 K, Figure 14. There is the opposite trend. From these data sets, we can assume that carbamazepine has lower interactions with polymer because the mobility in the mixtures is higher than that in

the pure state. The mobility of naproxen is always lower in mixtures, which is related to its stronger interactions with the polymer. The strength of the intermolecular interactions has a greater impact, meaning that paired molecules NAP-API slow the diffusion of other particles.

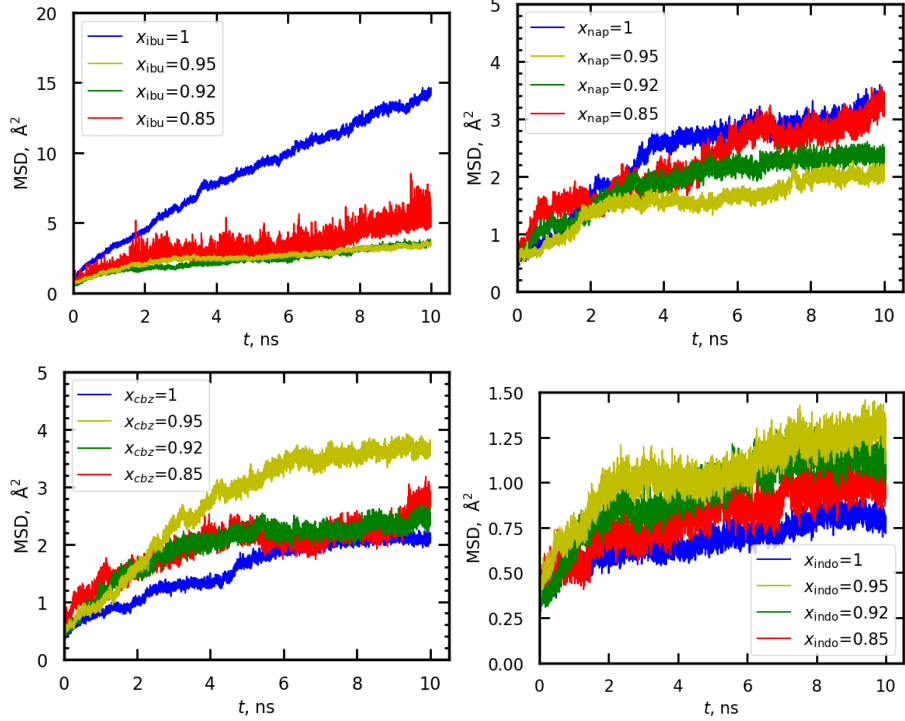


Figure 14: MSD from simulations under 300 K, ibuprofen (**top left**), naproxen (**top right**), carbamazepine (**bottom left**) and indomethacin (**bottom right**).

4.3 Smesi s polarizovanym polem

5 CONCLUSION

text

References

1. Leuner, C. Improving drug solubility for oral delivery using solid dispersions. *European Journal of Pharmaceutics and Biopharmaceutics* **2000**, *50*, 47–60.
2. Batisai, E. Solubility Enhancement of Antidiabetic Drugs Using a Co-Crystallization Approach. *ChemistryOpen* **2021**, *10*, 1260–1268.
3. Huang, L. Impact of solid state properties on developability assessment of drug candidates. *Advanced Drug Delivery Reviews* **2004**, *56*, 321–334.
4. Srinarong, P.; De Waard, H.; Frijlink, H. W.; Hinrichs, W. L. Improved dissolution behavior of lipophilic drugs by solid dispersions: the production process as starting point for formulation considerations. *Expert Opinion on Drug Delivery* **2011**, *8*, 1121–1140.
5. Vasconcelos, T.; Sarmento, B.; Costa, P. Solid dispersions as strategy to improve oral bioavailability of poor water soluble drugs. *Drug Discovery Today* **2007**, *12*, 1068–1075.
6. Caron, V.; Tajber, L.; Corrigan, O. I.; Healy, A. M. A Comparison of Spray Drying and Milling in the Production of Amorphous Dispersions of Sulfathiazole/Polyvinylpyrrolidone and Sulfadimidine/Polyvinylpyrrolidone. *Molecular Pharmaceutics* **2011**, *8*, 532–542.
7. Prudic, A.; Ji, Y.; Sadowski, G. Thermodynamic Phase Behavior of API/Polymer Solid Dispersions. *Molecular Pharmaceutics* **2014**, *11*, 2294–2304.
8. Newman, A.; Zografi, G. What Are the Important Factors That Influence API Crystallization in Miscible Amorphous API-Excipient Mixtures during Long-Term Storage in the Glassy State? *Molecular pharmaceutics* **2022**, *19*, 378–391, Place: United States.
9. Klajmon, M.; Aulich, V.; Ludík, J.; Červinka, C. Glass Transition and Structure of Organic Polymers from All-Atom Molecular Simulations. *Industrial & Engineering Chemistry Research* **2023**, *62*, 21437–21448.
10. Rainsford, K. D. Ibuprofen: pharmacology, efficacy and safety. *Inflammopharmacology* **2009**, *17*, 275–342.
11. Štejfa, V.; Pokorný, V.; Mathers, A.; Růžička, K.; Fulem, M. Heat capacities of selected active pharmaceutical ingredients. *The Journal of Chemical Thermodynamics* **2021**, *163*, 106585.
12. Drebushchak, T. N.; Boldyreva, E. V.; Mikhailenko, M. A. Crystal structures of sulfathiazole polymorphs in the temperature range 100–295 K: A comparative analysis. *Journal of Structural Chemistry* **2008**, *49*, 84–94.
13. Leach, A. R. *Molecular modelling : principles and applications*, 2nd ed.; Prentice-Hall International: Hemel Hempstead, UK, 1997.

- tice Hall Harlow, England: Harlow, England, 2001; Section: xxiv, 744 pages, 16 unnumbered pages of plates : illustrations (some color) ; 24 cm.
- 14. Monticelli, L.; Tieleman, D. P. In *Biomolecular Simulations*; Monticelli, L., Salonen, E., Eds.; Humana Press: Totowa, NJ, 2013; Vol. 924; p 197–213, Series Title: Methods in Molecular Biology.
 - 15. Vanommeslaeghe, K.; Guvench, O.; MacKerell, A. D. Molecular Mechanics. *Current Pharmaceutical Design* **2014**, *20*, 3281–3292.
 - 16. Da Silva, G. C. Q.; Silva, G. M.; Tavares, F. W.; Fleming, F. P.; Horta, B. A. C. Are all-atom any better than united-atom force fields for the description of liquid properties of alkanes? *Journal of Molecular Modeling* **2020**, *26*, 296.
 - 17. Nezbeda, I.; Kolafa, J.; Kotrla, M. *Úvod do počítačových simulací: metody Monte Carlo a molekulární dynamiky*; Karolinum, 1998.
 - 18. Thompson, A. P.; Aktulga, H. M.; Berger, R.; Bolintineanu, D. S.; Brown, W. M.; Crozier, P. S.; In 'T Veld, P. J.; Kohlmeyer, A.; Moore, S. G.; Nguyen, T. D.; Shan, R.; Stevens, M. J.; Tranchida, J.; Trott, C.; Plimpton, S. J. LAMMPS - a flexible simulation tool for particle-based materials modeling at the atomic, meso, and continuum scales. *Computer Physics Communications* **2022**, *271*, 108171.
 - 19. Martínez, L.; Andrade, R.; Birgin, E. G.; Martínez, J. M. PACKMOL: A package for building initial configurations for molecular dynamics simulations. *Journal of Computational Chemistry* **2009**, *30*, 2157–2164.
 - 20. Padua, A. ENS Lyon, France. <https://github.com/paduagroup/fftool>.
 - 21. Hockney, R.; Eastwood, J. *Computer Simulation Using Particles*, 0th ed.; CRC Press, 2021; p 540.
 - 22. Ryckaert, J.-P.; Ciccotti, G.; Berendsen, H. J. Numerical integration of the cartesian equations of motion of a system with constraints: molecular dynamics of n-alkanes. *Journal of Computational Physics* **1977**, *23*, 327–341.
 - 23. Tuckerman, M. E.; Alejandre, J.; López-Rendón, R.; Jochim, A. L.; Martyna, G. J. A Liouville-operator derived measure-preserving integrator for molecular dynamics simulations in the isothermal–isobaric ensemble. *Journal of Physics A: Mathematical and General* **2006**, *39*, 5629–5651.
 - 24. McAliley, J. H.; Bruce, D. A. Development of Force Field Parameters for Molecular Simulation of Polylactide. *Journal of Chemical Theory and Computation* **2011**, *7*, 3756–3767.
 - 25. Červinka, C.; Fulem, M. Structure and Glass Transition Temperature of Amorphous Dispersions of Model Pharmaceuticals with Nucleobases from Molecular Dynamics. *Pharmaceutics* **2021**, *13*, 1253.

26. Alzate-Vargas, L.; Fortunato, M. E.; Haley, B.; Li, C.; Colina, C. M.; Strachan, A. Uncertainties in the predictions of thermo-physical properties of thermoplastic polymers via molecular dynamics. *Modelling and Simulation in Materials Science and Engineering* **2018**, *26*, 065007.

List of Abbreviations

x position

v velocity

...

List of Symbols

x position

v velocity

...

List of Tables

1	The concentration of API in mixtures with PLA, expressed in molar and mass fractions.	12
2	Calculated mixing energies and volumes for API mixtures of different concentrations, simulations under 500 K.	13
3	Calculated mixing energies and volumes for API mixtures of different concentrations, simulations under 500 K.	14

List of Figures

1	PLA formula on the left, PLA dimer block representing the chain unit used to build up polymer chain in the middle and a folded PLA chain containing 100 dimer block used to create mixtures with APIs on the right.	2
2	Molecular structures of ibuprofen (top left), naproxen (top right), carbamazepine (bottom left) and indomethacin (bottom right). Atom types contributing most to the hydrogen bonding are tagged for each molecule.	4
3	Sulfathiazole - molecular structure on the left and a unit cell of its II polymorph on the right.	4
4	caption	6
5	Radial distribution function of the API-API interaction between HOIB hydrogen atom bonded on oxygen and OCIB oxygen atom in a mixture of ibuprofen and PLA for different concentration normalized on values for pure ibuprofen, temperature of 300 K in the left upper corner and 500 K bottom left, coordination numbers on the right. . .	15
6	Radial distribution function of the API-API interaction between HONP hydrogen atom and O2NP oxygen atom from COOH group in a mixture of naproxen and PLA for different concentration normalized on values for pure naproxen, temperature of 300 K in the left upper corner and 500 K bottom left, coordination numbers on the right. . .	16
7	Radial distribution function of the API-API interaction between HCZ6 hydrogen atom bonded on nitrogen and OCZ1 oxygen atom in a mixture of carbamazepine and PLA for different concentration normalized on values for pure carbamazepine, temperature of 300 K in the left upper corner and 500 K bottom left, coordination numbers on the right.	17
8	Radial distribution function of the API-API interaction between HCZ6 hydrogen atom and OCZ1 oxygen atom from COOH group in a mixture of indomethacine and PLA for different concentration normalized on values for pure indomethacine, temperature of 300 K in the left upper corner and 500 K bottom left, coordination numbers on the right.	18

Appendix A Headline